Optimization of a Planar "Bull-Eye" Leaky-Wave Antenna Fed by a Printed Surface-Wave Source

Symon K. Podilchak, *Member, IEEE*, Paolo Baccarelli, *Member, IEEE*, Paolo Burghignoli, *Senior Member, IEEE*, Al P. Freundorfer, *Senior Member, IEEE*, and Yahia M. M. Antar, *Fellow, IEEE*

***Abstract*—A microstrip-based leaky-wave antenna for two-sided frequency beam scanning and broadside radiation is presented. In particular, the optimized "bull-eye" ring structure is designed to support leakage of the fundamental TM mode of the guiding structure in a regime without any other leaky- or surface-wave modes. Also by following suggested design rules, to achieve good isolation between the printed rings and the TM source, a beam scan angle range of 121° can be realized over an operating bandwidth of more than 40% with antenna mismatch losses of less than 0.14 dB. Supporting numerical calculations are also in agreement with the simulations and antenna measurements.**

***Index Terms*—Leaky waves (LWs), leaky-wave antenna (LWA), surface waves (SWs).**

I. Introduction

THE DESIGN and analysis of planar leaky-wave antennas (LWAs) is a challenging topic and one of considerable interest [1]–[5]. These printed LWAs are generally attractive for radar and communication applications due to their low cost and ease of integration with other planar devices. In particular, two-sided frequency beam scanning in the upper xz-plane can be realized by a radial geometry of concentric ("bull-eye") microstrip rings [2]–[4] printed on a grounded dielectric slab (GDS) and excited by a slot in the ground plane. The design approach of such a "bull-eye" structure (Fig. 1) is based on the excitation of the fundamental TM_0 surface-wave (SW) mode of the GDS, which is in contrast to more classic topologies [6], [7], where antenna radiation is a result of the TE_1 mode.

In this letter a similar "bull-eye" structure is considered for TM leakage and TE field suppression, as in [2] and [3], but with an optimized microstrip grating (MSG) for wideband antenna operation. In particular, we improve our original LWA design [3] by optimally positioning the "bull-eye" grating with respect to the slot source positioned at the origin (see Fig. 1). We define this length as d_0, and it will be shown that by its proper selection, antenna performance can be improved. Results are supported by full-wave spectral analyses [8], HFSS simulations, and antenna measurements. For instance, antenna gain can be improved by 0.4 dB at broadside when compared to [3], while the radiating 3-dB bandwidth (BW) is enhanced from 1.68% to 2.23%. As further described, reduced cross-polarization levels are also observed, with respect to those reported in [3], as well as improved antenna matching and aperture efficiencies. Effectiveness of the design is also verified through Brillouin diagrams and dispersion analyses.

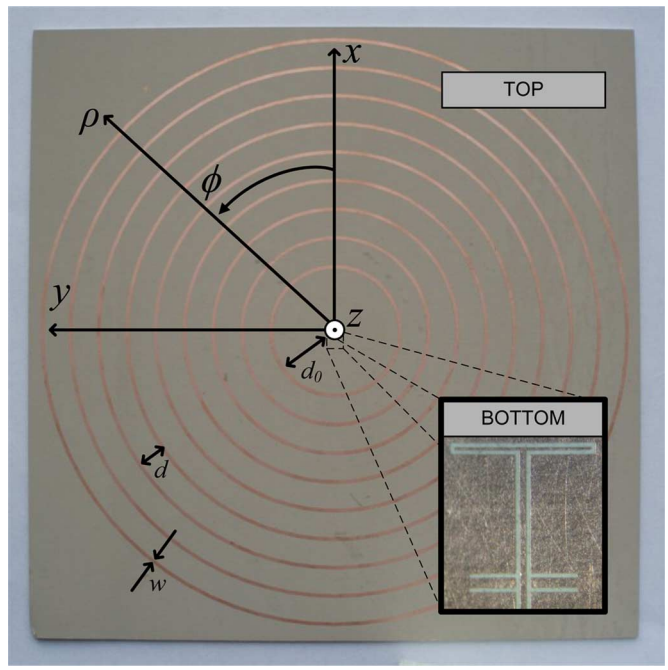

Fig. 1. Fabricated and measured "bull-eye" LWA under study with the TM SW source in the ground plane, as well as the 50-Ω coplanar waveguide feedline. LW radiation by the $n = -1$ spatial harmonic, which corresponds to Bragg diffraction of the incident TM SWs from the origin, occurs by the added metallic grating of periodicity $d = 8$ mm and strip width $w = 1$ mm, and placed at an optimized distance of $d_0 = 17.3$ mm from the origin.

II. Design Approach for Optimal TM Leakage

By the use of annular microstrip rings [2], the TM_0 SW fields generated from the main slot can excite cylindrical leaky-wave (LW) field distributions on the antenna guiding surface [9]. The modal analysis of such a "bull-eye" configuration is also based on an infinite 2-D structure with propagation normal to the strips [2]–[4].

Manuscript received April 10, 2013; revised May 07, 2013; accepted May 07, 2013. Date of publication May 13, 2013; date of current version May 30, 2013.

S. K. Podilchak and A. P. Freundorfer are with the Department of Electrical and Computer Engineering, Queen's University, Kingston, ON K7L 3N6, Canada (e-mail: symon.podilchak@queensu.ca; freund@queensu.ca).

P. Baccarelli and P. Burghignoli are with the Department of Information Engineering, Electronics and Telecommunications, Sapienza University of Rome, Rome 00184, Italy (e-mail: baccarelli@die.uniroma1.it; burghignoli@die.uniroma1.it).

Y. M. M. Antar is with the Department of Electrical and Computer Engineering, Royal Military College, Kingston, ON K7K 5L0, Canada (e-mail: antar-y@rmc.ca).

Color versions of one or more of the figures in this letter are available online at http://ieeexplore.ieee.org.

Digital Object Identifier 10.1109/LAWP.2013.2262572

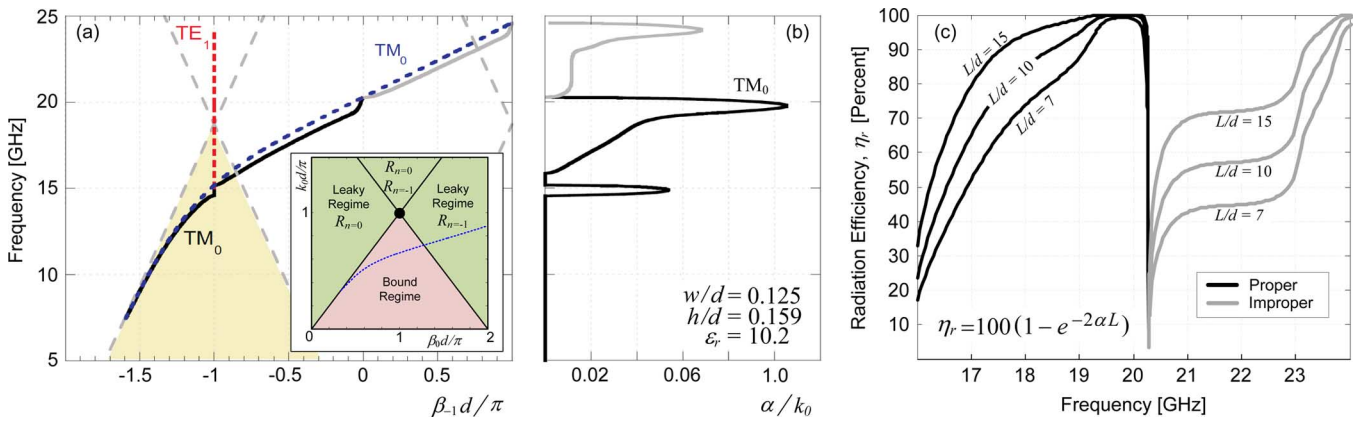

Fig. 2. (a) Brillouin diagram for the MSG (with period $d = 8$ mm and strip width $w = 1$ mm) printed on a GDS. The red (dashed), black (continuous), and gray (continuous) curves correspond to the $n = -1$ spatial harmonic of the perturbed TM and TE modes, while the (dashed) blue line corresponds to the fundamental (unperturbed) TM_0 SW mode. In addition, the bound and leaky regions, R_n, are shown in the inset (shaded red and green, respectively). (b) Attenuation constant for the perturbed TM_0 mode. (c) Radiation efficiency, $\eta_r = 100(1 - e^{-2\alpha L})$, for different antenna lengths L.

The Brillouin diagram for our proposed MSG ($d = 8$ mm, $w = 1$ mm) is shown in Fig. 2, as well as the LW attenuation constant for the radiating harmonic ($n = -1$) and its percentage radiation efficiency, η_r. Initially, the GDS was selected since the input power from the coplanar waveguide feedline can be efficiently coupled into the dominant TM_0 SW mode of the slab (with thickness $h = 1.27$ mm and $\varepsilon_r = 10.2$) by the slotted source in the antenna ground plane [3]. Values in Fig. 2 were numerically calculated using the method-of-moments (MoM) approach developed in [4], which rigorously takes into account the electromagnetic coupling among unit cells in the periodic structure.

To achieve TM_0 leakage in a regime without any other guided waves, parameters of the MSG were then selected such that the antenna operated in an LW regime with TE_1 SW suppression [3]. In particular, we designed the periodicity of the LWA such that at the cutoff frequency f_c for the TE_1 SW mode of the unperturbed (or unloaded) GDS, all the space harmonics of the MSG are in a leaky regime. This can be obtained by defining the antenna operating frequency f_0, such that $f_c > f_0$ (with $f_0 = c/2d$ and where c is the speed of light in vacuum). This corresponds to the tip of the bound triangle in the inset of Fig. 2(a), where $\beta d = \pi$ and $\beta = \omega/c$. We can also make use of a simple design equation that provides a minimum value for this grating periodicity [3]: $d > 2h\sqrt{\varepsilon_r - 1} = \lambda_c/2$ where λ_c is the free-space wavelength at the cutoff frequency f_c. Thus, by enforcing this design equation for the spatial periodicity, TE waves can be driven below cutoff in a regime where only the TM_0 LW mode is radiating. For practical realization of the finite LWA, the width of the strip ($w = 1$ mm) was also chosen to ensure that more than 80% of the power was radiated at broadside.

Following this GDS selection and design approach for the MSG, the TM_0 SW mode can be perturbed into a proper backward radiating LW from endfire to broadside [2]. The perturbed TE_1 SW mode is also shown in Fig. 2(a) for the same frequency range where it is in a stopband regime ($\beta_{-1}d = -\pi$). A small stopband also exists for the bound TM_0 SWs, but this is below the frequency range where the LWA radiates and is of little concern for antenna applications.

The LW open-stopband (OSB) region [1] for broadside radiating frequencies is shown from about 19.4 to 20.3 GHz in Fig. 2 where $\alpha > \beta$. At 20.3 GHz, the OSB frequency can be observed where the LW phase and attenuation constants are zero and this branch cut crossing defines no radiation from the structure [4]. However, for a practical MSG-GDS with material losses included (not shown for brevity), β passes through zero with α being nonzero, and consequently, sustained antenna leakage and continuous beam scanning [1]. Moreover, in this broadside radiating frequency range for such a two-sided LWA, the distinct beam patterns from endfire combine together to form a single pencil beam at broadside (at 19.4 GHz) where $\alpha \approx \beta$, followed by beam splitting and then continued two-sided beam scanning. Finally, it can be seen that with $L/d = 10$, high radiation efficiencies are achieved in a wide frequency range; note that for any value of L/d, the efficiency drops to zero at the OSB frequency where $\alpha = 0$.

III. Optimal Placement of the "Bull-Eye" Rings

An important design consideration is the optimal placement of the gratings with respect to the origin, i.e., the radius d_0 of the innermost ring (see Fig. 1). Although good antenna operation was achieved by the authors in [3] for $d_0 = 9.3$ mm, both azimuthally and radially directed current distributions were observed on the microstrip rings as seen from Fig. 3. Thus, operation for these antenna structures can be thought of as a superposition of the desired TM_0 LW field, which is related to the radially directed currents [3], as well as the azimuthally directed current distributions on the concentric rings that can diminish antenna performance.

After further investigations, and regardless of the selected spatial periodicity and strip width for TE suppression, it was found that the planar SW source employed within the antenna structure can also generate TE waves. Moreover, these TE waves, which are unwanted for the optimal "bull-eye" LWA examined in this work, can reflect power back toward the source diminishing the input match of the LWA structure, while also coupling energy into the metallic rings near the origin and generating the observed azimuthal current distribution.

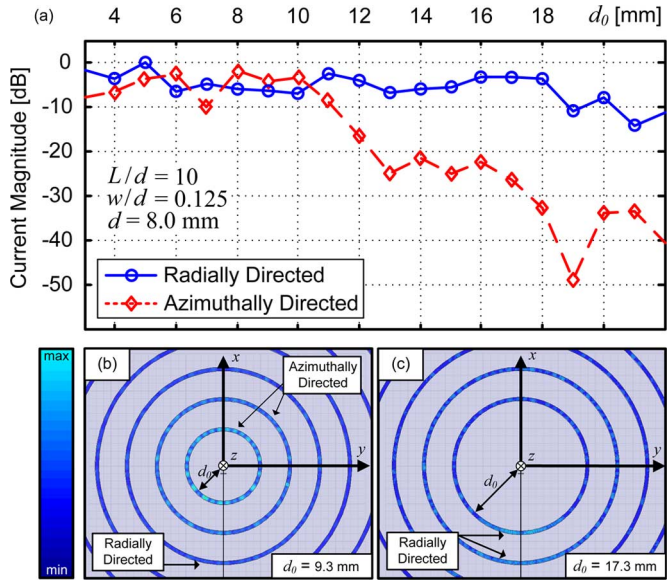

Fig. 3. (a) Simulated currents versus d_0 generated on the first ring at 22 GHz (in the middle of the strip and along the x-direction) for the proposed LWA structure and SWL with $L/d = 10$. (b), (c) Current distribution on the rings near the origin. For (b), $d_0 = 9.3$ mm [3], while (c) is the optimized structure in this work with $d_0 = 17.3$ mm (Fig. 1). In (b) [(c)], both radially and azimuthally directed [only radially directed] currents can be observed.

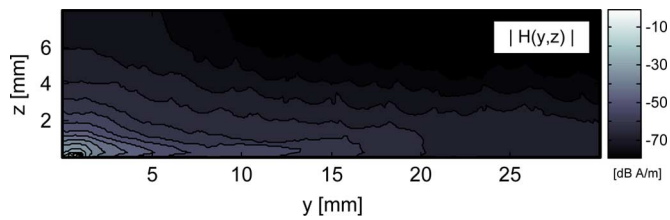

Fig. 4. Total magnetic field along the y-axis at 22 GHz generated by the bidirectional slot source placed at the origin ($z = 0$) and in the ground plane of the GDS. No circular gratings or strips were included in the simulation.

These TE waves originating from the planar source are mainly directed along the $\hat{y}$-axis and have a reduced field strength when compared to the $\pm x$-directed TM waves. By increasing the separation between the source and initial ring, i.e., by making $d_0 = 17.3$ mm, as in this letter, the unwanted azimuthal current distributions can be minimized as shown in Fig. 3. In particular, for d_0 values greater than 12 mm [17 mm] the difference between the magnitudes of the radially and azimuthally directed currents is greater than 10 dB [20 dB]. Physically speaking, increased isolation can be achieved between the microstrip rings and the planar source, and for such increased values of d_0, the magnetic field is consequently reduced in magnitude as well. For instance, as shown in Fig. 4, field values along the y-axis are decreased in amplitude by about 30 dB at this distance ($y = 17.3$ mm) and when compared to the total magnetic field at $y = 9.3$ mm.

Here, we further quantify our approach using a full-wave spectral analysis [8] to achieve a new design rule for d_0. First, we model the main driven slot of the planar SW source as an ideal magnetic dipole at the origin and in the ground plane, then the fields generated along the guiding surface and in the

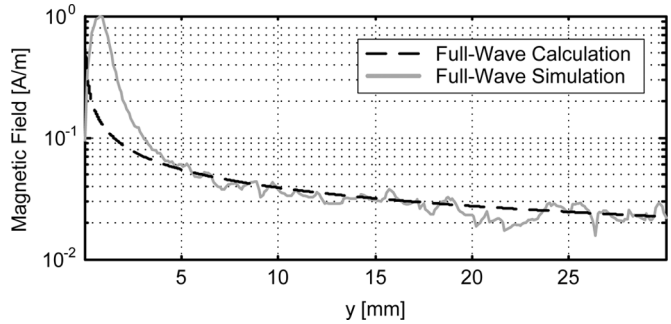

Fig. 5. Calculated magnetic field, $|H_z|$, at 22 GHz generated by the magnetic dipole antenna source. Field values shown along the y-axis and in the middle of the slab, $z = h/2$. This H_z field is representative of TE SWs generated by the planar source. Results are also compared to full-wave simulations.

absence of the metallic rings are determined. This analysis results in closed-form expressions for the z-oriented magnetic field vector, which corresponds to the excited TE waves incident onto the metallic rings. The TE$_z$ fields within the slab can be represented in an integral form as [8]

$$H_z = -\sin\phi \frac{jK}{2\pi\omega\mu_0} \int_0^\infty H_1^{(2)}(k_\rho \rho)\, g(k_\rho; z)\, k_\rho^2\, dk_\rho \quad (1)$$

where K is the magnetic moment of the slot source (in V·m) and $H_1^{(2)}$ is the Hankel function of the second kind (order 1). The spectral function $g(k_\rho; z)$ characterizes the fields within the guiding surface and has poles that define the TE SW modes of the GDS. By applying boundary conditions, $g(k_\rho; z)$ can be further established

$$g(k_\rho; z) = \cos(k_{z1} z) - jb(k_\rho)\sin(k_{z1} z)$$
$$\text{where } b(k_\rho) = \frac{k_{z0}\cos(k_{z1}h) + jk_{z1}\sin(k_{z1}h)}{k_{z1}\cos(k_{z1}h) + jk_{z0}\cos(k_{z0}h)} \quad (2)$$

and $k_{zi}^2 = k_i^2 - k_\rho^2$ with $k_i^2 = \omega^2\mu_0\epsilon_i$ (where $i = 0$ and $i = 1$ refer to the air and dielectric regions, respectively). Now the H_z field can be determined along the $\hat{y}$-direction for TE SWs by evaluating the residue contribution of the relevant SW pole

$$H_z(y) = \frac{K}{\omega\mu_0} \left. \frac{N(k_\rho)}{\frac{\partial D(k_\rho)}{\partial k_\rho}} \right|_{k_\rho = \beta}. \quad (3)$$

In (3), β refers to the phase constant for the TE$_1$ SW mode of the GDS, whereas $N(k_\rho)$ and $D(k_\rho)$ are the numerator and denominator of the integrand in (1), with the time-dependent term $(e^{+j\omega t})$ suppressed throughout.

Numerical calculations for $H_z(y)$ are shown in Fig. 5, and good agreement is shown with the full-wave simulations for $y > 5$ mm. The deviations at the origin are expected and are related to the finite length of the main slot of the bidirectional TM SW source ($\approx\lambda_0/2\sqrt{\varepsilon_r}$), as the analysis assumed an infinitely small magnetic dipole. Regardless, good agreement is observed for $y \gg 0$, and thus the derived H_z field distribution in (3) is representative of the TE waves along the $\hat{y}$-axis.

The design equation for positioning of the innermost ring can be developed. Moreover, to achieve good isolation between the planar source and the radiating "bull-eye" aperture, a value for d_0 and the grating periodicity d should be chosen such that

TABLE I
FABRICATION DETAILS AND MEASURED RADIATION CHARACTERISTICS

	$d_0 = 9.3$ mm [3]	$d_0 = 17.3$ mm
Antenna Dimensions :		
Total Substrate Size	170 mm by 170 mm	170 mm by 170 mm
Optimized Periodicity	$d = 8$ mm	$d = 8$ mm
Strip Width	$w = 1$ mm	$w = 1$ mm
Antenna Length	$L/d = 10$	$L/d = 9$
Aperture Area, a	$25,052.6$ mm^2	$25,052.6$ mm^2
Two-Sided Patterns :		
Radiating Frequency BW	38.30 %	41.51 %
Gain Variation	19.1 dB	18.5 dB
Antenna Match	VSWR < 1.92	VSWR < 1.45
Broadside Pencil-Beam :		
Maximum Gain, G_{max}	13.1 dBi	13.5 dBi
Radiating BW, 3 dB	1.68 %	2.23 %
Aperture Efficiency, η_a	1.84 %	2.02 %
Cross-Polarization Level	< 18.0 dB	< 20.6 dB
Antenna Match	VSWR < 1.85	VSWR < 1.35

Note: Comparison of LWAs presented in [3] ($d_0 = 9.3$ mm) and this work ($d_0 = 17.3$ mm) where the physical aperture area, a $(= \pi(L + d_0)^2)$ was maintained. The aperture efficiency, η_a, was calculated using the maximum realized gain, G_{max}, observed at 17.8 GHz for both LWAs, with $\eta_a = G_{max}(\lambda_0 / 2\pi(L + d_0))^2 = G_{max}\,\lambda_0^2/(4\pi a)$.

$|H_z(y = d_0)| \approx |H_z(y = d)|/\sqrt{2}$. According to this approximation, we are ensuring that the absolute value of the field strength at $|H_z(y = d_0)|$ is about 3 dB below the reference field $|H_z(y = d)|$. Mainly, we are trying to minimize the generation of any azimuthally directed currents on the printed rings by attempting to reduce the electromagnetic coupling between the TE waves generated by the planar source and the MSG. This is possible due to the decreased magnetic field strength (and consequently minimized azimuthal current distribution) for $d_0 > 2d$ when compared to field values closer to the origin, $d_0 \leq d$ for example, as shown in Figs. 3–5.

It should also be noted that we are defining the reference magnetic field $|H_z(y = d)|$ at $y = d$ since this dimension is comparable to the wavelength of antenna operation, while it also defines the spatial periodicity of our designed structure. Furthermore, d_0 should not be too large; i.e., $d_0 < 3\,d$ as to not increase the size of the guiding surface and to not diminish the aperture efficiency of the LWA. For instance, consider a radiating aperture having an antenna length L and periodicity d $(=$ 8 mm) such that $L/d = 10$. The aperture efficiency $\eta_{\rm a}$ has been calculated considering an ideal 2-D LWA [9] with LW phase and attenuation constants as computed for the optimized MSG [see Fig. 2(a) and (b)]. At 22 GHz, $\eta_{\rm a}$ can decrease by 0.251% for $d_0 = 2d$ [0.608% for $d_0 = 3d$] $\langle 0.925\%$ for $d_0 = 5d\rangle$ when compared to $d_0 = d$. Other values for d_0 were investigated for our LWA prototype, but the presented length for d_0 $(= 17.3\,\text{mm} > 2d) \approx 2d + w \approx \lambda_0$ offered the best result in terms of reduced antenna size and minimal currents that were directed along the azimuthal direction. This also provides a suitable comparison to the measured LWA in [3] mainly since all dimensions for the LWA in this work were selected to maintain a common periodicity, strip width, and physical aperture size to that of [3] as outlined in Table I.

IV. ANTENNA MEASUREMENTS AND DISCUSSIONS

The proposed LWA structure was fabricated and measured in a calibrated anechoic chamber. Results are reported in Figs. 6–9 and Table I. In particular, good agreement is observed between the full-wave simulations and the predicted pointing angle using the MoM dispersion analysis [4] as shown in Fig. 6. However, there is a downward shift in frequency (≈2 GHz) that can be related to anisotropic effects of the electrically thick substrate. In particular, for some substrates, the dielectric constant in the vertical direction can be different than that in the horizontal direction, and thus a tensor can be used to model the material [10], [11]. This anisotropy can be significant for thick substrates, is a result of manufacturing, and as suggested in [10], has a frequency dependence. It can also be modeled using an increased value for the dielectric constant of the GDS. Nevertheless, agreement is shown between the measurements, full-wave simulations, and the MoM dispersion analysis.

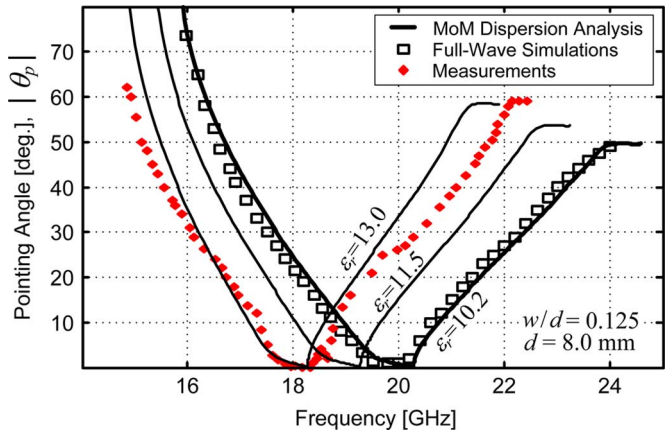

Fig. 6. Absolute value of the pointing angle, $|\theta_p|$, for the optimal "bull-eye" LWA investigated in this letter. Similar downward frequency shifts have been observed by the authors and can be modeled with an increased $\varepsilon_{\rm r}$ by [10].

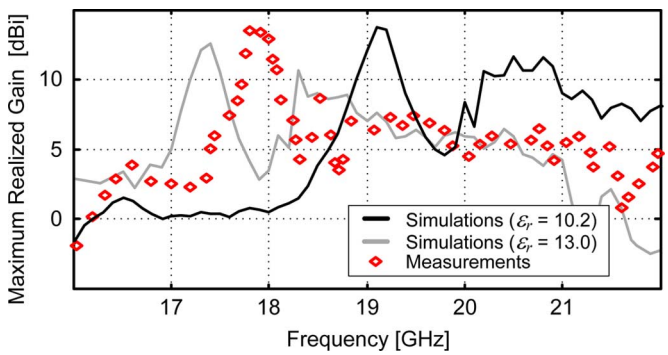

Fig. 7. Measurements and full-wave simulations of the maximum realized gain in the E- (xz-) plane as a function of frequency.

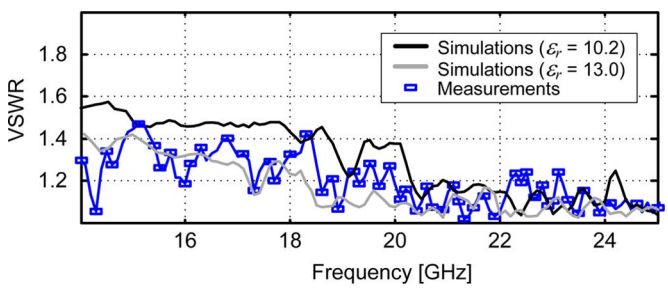

Fig. 8. Measured VSWR compared to simulations for $\varepsilon_{\rm r} = 10.2$ and 13.0.

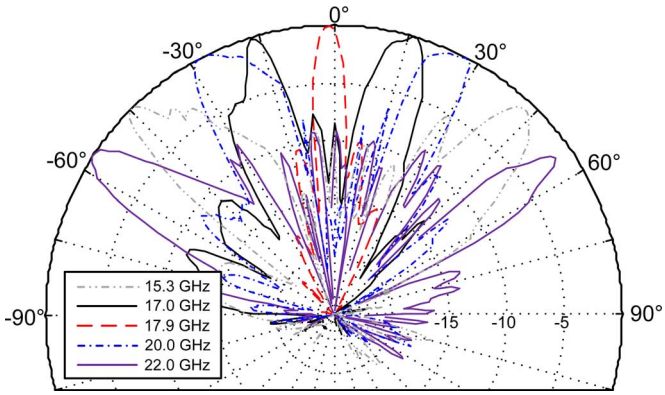

Fig. 9. Measured two-sided and broadside beam patterns in the E- (xz-) plane. Patterns were normalized to the observed maximum at each frequency.

Improved gain values and reduced reflection losses are also observed for our proposed LWA structure ($d_0 = 17.3$ mm) when compared to [3] ($d_0 = 9.3$ mm). In particular, the gain variation was decreased by 0.6 dB for our optimized LWA, while the operational BW, where frequency beam scanning was observed, was enhanced from 38.30% to 41.51% when compared to [3]. In addition, the aperture efficiency at broadside and the radiating BW (3 dB) improved by 0.6% and 0.2%, respectively. These results suggest that the design schemes for the positioning and the spatial periodicity of the MSG can indeed improve LWA performance and, in particular, that a unimodal guiding structure can be designed to achieve leakage of the fundamental TM_0 SW mode over a large BW.

Maximum gain values of 13.5 dBi at 17.8 GHz were also shown in this letter with $|S_{11}| < -15$ dB, while in [3], a reduced broadside gain (13.1 dB) was reported with $|S_{11}| < -10$ dB at this same frequency. The desired two-sided beam patterns, along with broadside radiation, are observed in Fig. 9 for our optimized LWA structure. In particular, wide-angle beam scanning is also shown over a 7.7-GHz radiating BW; i.e., $\theta_p \in [-62°, +59°]$ from 14.7 to 22.4 GHz as in Fig. 6.

V. Conclusion

A printed "bull-eye" LWA structure was designed for two-sided frequency beam scanning and directive radiation at broadside. In particular, by selection of an optimized grating periodicity for the employed GDS, leakage of the fundamental TM_0 SW mode can occur when the TE_1 SW mode of the slab is suppressed. Simple design rules for the periodicity and optimal placement of the microstrip rings are also provided in that a value of $d_0 \approx \lambda_0$ is convenient to reduce the near-field coupling produced by the feed element to that of the MSG. When compared to previously examined LWAs [3], the radiating 3-dB BW is improved from 1.68% to 2.23%, while the power gain is enhanced by 0.4 dB at broadside. The input match is also improved (VSWR of 1.35 from 1.85 [3]) for the optimized LWA. Results are further supported by Brillouin diagrams and full-wave analyses.

References

[1] P. Burghignoli, G. Lovat, and D. R. Jackson, "Analysis and optimization of leaky-wave radiation at broadside from a class of 1-D periodic structures," *IEEE Trans. Antennas Propag.*, vol. 54, no. 9, pp. 2593–2604, Sep. 2006.

[2] P. Baccarelli, P. Burghignoli, G. Lovat, and S. Paulotto, "Novel microstrip leaky-wave 'bull-eye' antenna with suppressed surface-wave excitation," in *Proc. IEEE AP-S Int. Symp.*, 2004, vol. 1, pp. 1078–1081.

[3] S. K. Podilchak, Y. M. M. Antar, A. P. Freundorfer, P. Baccarelli, P. Burghignoli, S. Paulotto, and G. Lovat, "Planar antenna for continuous beam scanning and broadside radiation by selective surface wave suppression," *Electron. Lett.*, vol. 46, no. 9, pp. 613–614, Apr. 2010.

[4] P. Baccarelli, P. Burghignoli, F. Frezza, A. Galli, P. Lampariello, G. Lovat, and S. Paulotto, "Modal properties of surface and leaky waves propagating at arbitrary angles along a metal strip grating on a grounded slab," *IEEE Trans. Antennas Propag.*, vol. 53, no. 1, pp. 36–46, Jan. 2005.

[5] M. Ettorre, S. Bruni, G. Gerini, A. Neto, N. Llombart, and S. Maci, "Sector PCS-EBG antenna for low-cost high-directivity applications," *IEEE Antennas Wireless Propag. Lett.*, vol. 6, pp. 537–539, 2007.

[6] I. A. Encinar, "Mode-matching and point-matching techniques applied to the analysis of metal-strip loaded dielectric antennas," *IEEE Trans. Antennas Propag.*, vol. 38, no. 9, pp. 1405–1412, Sep. 1990.

[7] M. Guglielmi and D. R. Jackson, "Broadside radiation from periodic leaky-wave antennas," *IEEE Trans. Antennas Propag.*, vol. 41, no. 1, pp. 31–37, Jan. 1993.

[8] J. R. Wait, *Electromagnetic Waves in Stratified Media*. New York, NY, USA: Pergamon, 1962, ch. 2.

[9] A. Ip and D. R. Jackson, "Radiation from cylindrical leaky waves," *IEEE Trans. Antennas Propag.*, vol. 38, no. 4, pp. 482–488, Apr. 1990.

[10] R. Garg, P. Bhartia, I. Bahl, and A. Ittipiboon, "App. A," in *Microstrip Antenna Design Handbook*. Norwood, MA, USA: Artech House, 2001.

[11] D. Pozar, "Radiation and scattering from a microstrip patch on a uniaxial substrate," *IEEE Trans. Antennas Propag.*, vol. AP-35, no. 6, pp. 613–621, Jun. 1987.